Brillouin light-scattering observation of the nonlinear spin-wave decay in yttrium iron garnet thin films

Hong Yan Zhang,* Pavel Kabos,† Hua Xia,‡ Pavel A. Kolodin,§ and Carl E. Patton
Department of Physics, Colorado State University, Fort Collins, Colorado 80523
(Received 24 June 1999)

The direct observation of nonlinear spin-wave decay in thin yttrium iron garnet (YIG) films is reported. The second-order parametric spin waves were excited by a series of nonlinear magnetostatic backward volume wave (MSBVW) pulses propagated in a microstrip structure at 5 GHz. Brillouin light-scattering techniques were used to detect spin waves in the YIG at a point along the propagation path. Data were obtained as a function of the input pulse duty cycle and peak power level. These data yielded the decay rate η_{eff} for the parametric spin waves vs input power P_{in}. This η_{eff} was equal to the usual spin-wave relaxation rate at low power, but decreased rapidly with increasing P_{in}. As P_{in} approached the threshold power for complete MSBVW soliton formation at the observation point, η_{eff} leveled off to a relatively constant value that was about a factor of 5–10 smaller than the low power value. The initial decrease in η_{eff} with power is due to the compensation of the usual spin-wave decay by the simultaneous parametric pumping of the spin waves by Suhl processes. The leveling off in η_{eff} at the soliton threshold is due to the spin-wave shedding that is needed to maintain order one eigenmode soliton propagation at high input power levels. These experiments demonstrate the reduction in the spin-wave decay rate with power *below* the threshold for spin-wave instability. This reduction is a key element in spin-wave instability theory that has never been observed directly. The data also demonstrate the enhanced production of parametric spin waves that accompanies microwave magnetic envelope soliton formation.

I. INTRODUCTION

The discovery of microwave magnetic envelope (MME) soliton generation in magnetic films was reported over a decade ago.[1–3] Since these initial reports, a substantial experimental and theoretical effort has been devoted to the study of MME pulse propagation and soliton formation in yttrium iron garnet (YIG) films. This work has addressed soliton propagation and decay,[4–7] dark solitons,[8,9] soliton order and a power-dependent soliton velocity,[10,11] soliton phase profiles,[12] soliton modeling based on the nonlinear Schrödinger equation and inverse scattering considerations,[13,14] feedback generated solitons,[15,16] the parametric amplification of MME solitons,[17,18] and the Brillouin light-scattering (BLS) detection of soliton wave-vector distributions,[19] and the spatio-temporal power distributions of soliton bullets.[20]

The Brillouin light-scattering measurements of the wave-vector distributions for the magnetic excitations associated with MME solitons in Ref. 19 revealed more than the expected Fourier transform makeup of the nonlinear MME wave packet. These data indicated that soliton formation, propagation, and decay was accompanied by the generation of high-wave-number spin waves. The detected spin waves included excitations with wave number k much larger than $1/S$, where S is the spatial width of the soliton pulse. The wave-number k distribution for the scattered spin waves was sharply peaked around $k=3-4\times10^4$ rad/cm, and shown to evolve from a broad k distribution for cw microwave excitation as found in Ref. 21. These high-k modes had discrete wave-vector directions that were perpendicular to the propagation direction and at angles at about 22°–23° and 45° away from perpendicular. Such soliton generated spin waves are consistent with the evidence of a wake signal that follows an MME soliton found from soliton collision experiments.[6]

Reference 19 provided two suggestions about the origin of the high-wave-number spin waves produced during soliton propagation. The first involved a possible shedding of energy in the form of spin waves as the initial rectangular input magnetostatic wave (MSW) pulse signal evolves into an eigenmode envelope soliton. The second was the generation of spin waves through parametric Suhl processes.[22] The fact that the spin waves gave maximum scattering for a wave number k around $3-4\times10^4$ rad/cm and for discrete in-plane wave-vector directions is very suggestive of the sort of critical mode considerations associated with Suhl processes.

The realization that MSW soliton pulses generate high-wave number spin waves during propagation and that these spin waves have many of the characteristics of the parametric excitations found in Suhl processes poses an interesting possibility—the direct measurement of the spin-wave relaxation rate. Such a determination can be made quite easily from data on the BLS scattering intensity at a localized point along the MSW pulse propagation path. All that is needed is to measure the cw BLS intensity as a function of the duty cycle for the MSW pulse excitation. There is no need for the nanosecond scale temporal resolution of the scattered light described in Ref. 20. The technique will be described in Sec. II.

The results are presented in Sec. III. They turn out to be rather surprising. If the generation of spin waves is intrinsic to the soliton formation process, one should see scattering from such modes as soon as one exceeds the power threshold for soliton formation. The decay rate for these excited modes, moreover, should correspond to the intrinsic spin-wave relaxation rate η_k. The data show that the measured

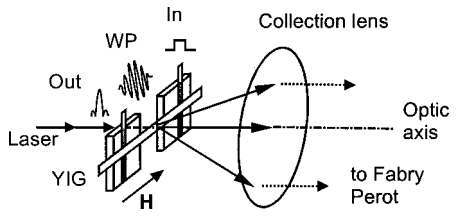

FIG. 1. YIG film transducer structure and optical configuration for the BLS spin-wave measurements.

spin-wave relaxation rate does start out at this intrinsic η_k value for low-power input pulses. As the input power is increased, however, the spin-wave relaxation rate *decreases rapidly*, and levels off at a small value of about a factor of 5–10 smaller than η_k as one approaches and exceeds the input power needed for complete order one soliton formation at the output antenna for the MSW delay line structure.

These data show that the effective decay rate for the soliton pumped spin waves is not the intrinsic spin-wave relaxation rate at all. Rather, the excited spin waves appear to decay much slower as one approaches some critical power threshold for spin-wave instability, as found for Suhl processes, and then saturate as one exceeds the power needed for complete soliton formation at the point of observation. The possible basis for these unexpected results in spin-wave instability processes[22,23] will be considered in Sec. IV.

II. EXPERIMENT AND RELAXATION RATE DETERMINATION

The microwave/optical system is shown schematically in Fig. 1. The experiment used a long, 2-mm-wide, 7.2-μm-thick YIG film grown by liquid phase epitaxy and a special open-design microstrip transducer structure for microwave excitation and simultaneous microwave and optical detection. The film had a 10-GHz ferromagnetic resonance linewidth below one Oe and magnetostatic wave transmission profiles indicative of unpinned surface spins. The YIG film strip is shown positioned across the two 50-μm-wide transducer sections in Fig. 1, one for input and one for output. The propagating MSW wave packet (WP) is also indicated. The static magnetic field H was aligned parallel to the long dimension of the YIG film and the MSW propagation direction. This corresponds to the magnetostatic backward volume wave (MSBVW) configuration.[24]

The input microwave pulse signals were obtained with a microwave synthesizer followed by a high speed microwave switch, a microwave amplifier, and an attenuator. The pulse carrier frequency was set at 5 GHz. The field H was adjusted so that the MSBVW pulses at low power had a group velocity v close to 3.5×10^6 cm/s. This corresponds to an MSBVW carrier wave number k close to 100 rad/cm. These relatively long-wavelength MSW signals could be excited and detected efficiently by the 50-μm-wide microstrip transducer elements. The nominal field H for these MSW operating-point conditions was 1090 Oe. All experiments were done with an input pulse width of 20 ns.

Although Fig. 1 shows single pulses at input and output, the experiments were done with continuous pulse trains rather than single-shot pulses. The pulse repetition period could be varied from 0.2 to 4 μs, corresponding to a variation in duty cycle from 10% to 0.5%. As will be discussed shortly, the duty cycle for the microwave input pulse train signal is a critical control parameter for the spin-wave decay time measurements. The microwave signals were analyzed through a Hewlett Packard HP71500A Microwave Transition Analyzer.

The microwave system could also be used to perform accurate measurements of the MME pulse velocity, decay rates, and output pulse peak power.[4,7,11] These data were obtained as a function of pulse power and duty cycle. The duty cycle had no effect on the output pulse response. Increasing power resulted in the usual nonlinear output power response, change in pulse shape, change in decay rate, and change in pulse velocity associated with MME solitons. These effects are described in the references cited above.

The BLS measurements utilized an optical system set up in the forward scattering configuration, and a Sandercock six-pass tandem Fabry-Perot interferometer[25] for the detection of spin-wave scattered light. The BLS set up was essentially the same as in Ref. 19, except that there were no wave-vector selection slits or irises in the collection optics. With no wave-vector selective apertures, the BLS system collects essentially all of the scattered light within the lens aperture and routes this light signal to the Sandercock Fabry-Perot interferometer. The BLS data were obtained for an incident laser power level of about 10–15 mW. The upper limit on the accessible spin-wave wave number was about 3×10^4 rad/cm.

Care was taken to obtain BLS data and microwave data corresponding to one and the same area of the YIG film along the propagation path. In order to do this, the movable output antenna was first positioned at the distance of 3 mm from the input antenna, and microwave data were obtained. Then, the output antenna was moved to a distance of 6 mm from the input antenna to monitor the microwave signal during the BLS data collection, and the incident laser beam was focused in the middle of the YIG film strip at the same position used for the previous microwave data collection. In this way, one obtains BLS data and microwave data for the same location along the MSW pulse propagation path from input to output.

The spin-wave decay measurements are based on two simple assumptions. First, it is assumed that the propagating MME magnetostatic wave pulse serves to excite spin waves locally at all points along the propagation path and, in particular, at the point of observation for the BLS signal. The relatively low-wave-number MSW pulse serves the same role as the uniform mode ferromagnetic resonance signal in the standard Suhl resonance saturation experiment. For such experiments, the generation of parametric spin waves is well established.[21] The second assumption is that these spin waves that are excited as the MSW pulse passes the point of observation will decay following this passage and exhibit a characteristic decay with time. This decay may be written as

$$S_k \propto e^{-\eta_{\mathrm{eff}} t}, \tag{1}$$

where S_k represents the spin-wave signal level, η_{eff} represents the decay or relaxation rate for the excited spin waves, and t represents the time referenced to the time at which the MSW pulse passes the BLS observation point.

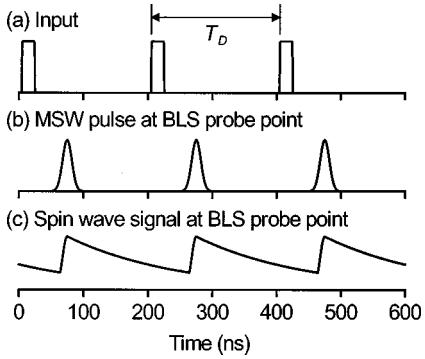

FIG. 2. Schematic diagram of the pulse timing for the BLS detection of decaying spin-wave signals after excitation by the MSW pulses. Trace (a) shows the repetitive train of microwave input pulses, trace (b) shows the delayed train of MSW pulses at the BLS probe point, and trace (c) shows the expected time-dependent spin-wave signal level at the BLS probe point.

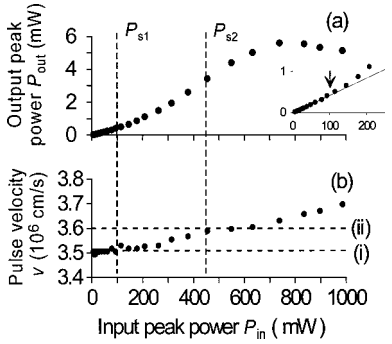

FIG. 3. Graph (a) shows typical data on the output peak detected power P_{out} vs input peak power P_{in} for the 20-ns MSBVW pulses in the 7.2-μm-thick YIG film with a transducer spacing of 3 mm. Graph (b) shows the average pulse velocity vs P_{in}. The static magnetic field was 1090 Oe. The input pulse carrier frequency and width were 5 GHz and 20 ns, respectively.

The time sequencing for the input and propagating pulse signals and the form of the transient spin-wave signal are shown schematically in Fig. 2. The horizontal time scale and pulse profiles are more-or-less representative of the data, with 20-ns-wide input pulses, somewhat narrowed soliton pulses at the BLS observation point, and a spin-wave decay time of about 170 ns/rad. The pulse spacing or duty cycle period T_D is shown as 200 ns. This is at the lower limit of the duty cycle period used in the measurements. Trace (a) shows the repetitive input pulse and trace (b) shows the MSW pulse at the BLS observation point. These traces represent observable microwave signals. Trace (c) shows the expected transient population of the parametrically pumped spin waves at the BLS observation point as well. The decay shown in (c) corresponds to typical the intrinsic spin-wave decay rates.

Note that the MSW pulses in (b) and the peaks in the transient response in (c) are displaced in time from the input pulse timing points. This displacement is due to the group velocity for the MSW pulses. For the MSBVW group velocity of 3.5×10^6 cm/s and the 3-mm transducer separation for the experiment, the corresponding MSW pulse travel time is about 85 ns.

It is clear from Fig. 2 that as the duty cycle period T_D is increased, the average spin-wave signal will decrease. If one neglects the finite-time spin-wave response at the beginning of the MSW pulse signals and assumes a simple-step increase each time the MSW pulse passes the BLS observation point, and further assumes that the measured BLS intensity I_{BLS} is proportional to the time-averaged spin-wave signal level, one obtains a simple expression for the BLS intensity—duty cycle period product $I_{BLS}T_D$,

$$I_{BLS}T_D = C(1-e^{-\eta_{eff}T_D})+B. \tag{2}$$

The parameter C relates to the light intensity, the MSW pulse shape and amplitude, and the corresponding coupling to the spin waves. The B parameter relates to any BLS signal due to the low-wave-number Fourier component spin waves that make up the MSW pulse itself. Note that the photo detector in the BLS system essentially collects the photons that are scattered by the magnetic excitations present at the point of observation, so that I_{BLS} derives from the average spin-wave signal or the time average of the response shown in Fig. 2(c).

Equation (2) demonstrates the basic principle behind the spin-wave decay-rate measurements. Namely, if all the pulse conditions are maintained constant except the duty cycle, one can use time averaged BLS data as a function of duty cycle period to obtain a direct determination of the decay rate. The only practical requirement for a meaningful measurement of η_{eff} from a sequence of *time-averaged* BLS measurements is that the incident light intensity, the input pulse power and width, and the total collection time remain constant.

As noted above, the B term in Eq. (2) is associated with any BLS signal due to the low-wave-number magnons associated with the MSW pulse itself. This signal would amount to an additional scattering that would just coincide with the MSW pulses in trace (b) of Fig. 2. For such scattering, if present, it is reasonable to assume that the time-averaged BLS signal would scale with the pulse power and $1/T_D$. The effect of such scattering, therefore, would be simply to add the constant B term on the right-hand side. This direct MSW pulse scattering has no effect on the exponential decay T_D term in Eq. (2). The extent of such scattering, as well as the validity of the simple spin-wave decay model described above and corresponding relaxation-rate determination, can be tested through BLS intensity measurements as a function of the duty cycle period T_D. Such data are considered below.

III. EXPERIMENTAL RESULTS

A. MSW pulse-power response characteristics

Before considering the duty cycle results, it will be useful to consider first the MSW pulse-power response characteristics at the BLS observation point. As discussed in Refs. 4 and 11, the output peak power vs input power profile and the change in the average pulse group velocity with power allow one to clearly define the pulse experiment. Such data serve to identify the threshold power for the onset of soliton formation and the input power needed for complete order one soliton formation.

Figure 3 shows representative data on (a) the MSW output peak power P_{out} vs the input peak power P_{in} and (b) MSW pulse velocity vs P_{in} for the transducer structure and

YIG film combination used for the BLS spin-wave decay measurements. As noted in Sec. II, these data were obtained with the output microstrip transducer positioned 3 mm from the input transducer, the same as the probe point for the BLS measurements. Of course, the details of the responses shown in Fig. 3 will change if the transducer separation is changed. The inset in (a) shows the initial P_{out} vs P_{in} response on an expanded scale, along with a linear fit to the data at very low input peak powers. The vertical dashed lines identify characteristic threshold power points P_{s1} and P_{s2} for solitons that will be important in the interpretation of the spin-wave decay-rate data. The two horizontal dashed lines in (b) indicate (i) the limiting pulse velocity in the low power limit and (ii) the slightly higher velocity plateau for order one solitons.

Graph (a) shows the typical P_{out} vs P_{in} power profile associated with MME solitons in magnetic films. First, there is the initial linear response at input peak powers below about 100 mW. The arrow in the inset shows this subtle but distinct 100-mW transition point from a linear to a nonlinear response. Above $P_{in}=P_{s1}=100$ mW, there is a growing deviation from the linear response as the soliton formation process begins. Then, for P_{in} above about 800 mW, there is a falloff in the response when the power is sufficient to generate higher-order solitons.[10,13]

Graph (b) shows the small but distinct change in pulse velocity that accompanies soliton formation.[7] With the onset of the soliton formation process for power levels above $P_{in}=P_{s1}$, the average pulse velocity increases from the baseline low power linear MSBVW pulse velocity. At the power indicated by P_{s2}, this small but distinct increase in the pulse velocity pauses momentarily and then resumes the gradual increase above this second P_{s2} baseline. The power level $P_{in}=P_{s2}=450$ mW may be taken as the power threshold for complete order one soliton formation at the 3-mm detection point.

The intrinsic spin-wave relaxation rate η_k will play an important role in Secs. III B and IV. Two low-power measurements, one of the ferromagnetic resonance linewidth and one of the spatial decay rate for the MSW pulses, were been used to determine η_k independent of the duty cycle results. These measurements place η_k at about 6×10^6 rad/s for long-wavelength MSW signals at 5 GHz. Direct microwave cavity spin-wave instability threshold measurements for parallel pumping at 10 GHz, properly scaled for the factor of 2 increase in frequency, also give an η_k value in this same range.

B. Spin-wave decay measurements

For the spin-wave decay measurements, BLS data were obtained at a point 3 mm from the input transducer for a range of duty cycle periods from 0.2 to 4 μs. The input microwave pulse width was maintained at 20 ns for all of the measurements. For each T_D setting, data were obtained at a fixed level of the microwave input power and with the multichannel acquisition time, incident light intensity, and other BLS collection parameters also held constant. Such data were obtained for a range of input peak power levels from a few tens of mW to 1.6 W. These power levels covered the entire range of powers used in microwave measurements. Figure 4 shows a series of typical results from the measurements of the BLS intensity I_{BLS} as a function of the duty cycle period T_D. The five graphs show data in the format suggested by Eq. (2), namely, plots of the $I_{BLS}T_D$ product as a function of T_D. From top to bottom, the graphs are for increasing input peak power P_{in} levels. These levels range from 5 mW for the top panel, a value well below the $P_{s1}=100$ mW threshold in Fig. 3(a), to 1650 mW for the bottom panel, a value well beyond the P_{s2} point in Fig. 3(b) and the broad peak in the output peak power response in Fig. 3(a). The graphs show no vertical scales, since the BLS collection parameters varied somewhat from run to run. For a given run, of course, these settings were maintained constant. The solid curves in the graphs represent best fits to the respective data based on the functional response in Eq. (2).

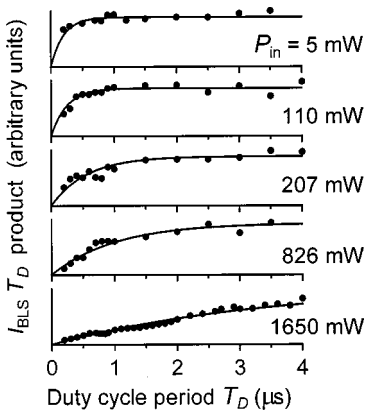

FIG. 4. Graphs of the product of the time-averaged BLS intensity I_{BLS} and the duty cycle period T_D as a function of the duty cycle period for a series of increasing input peak power P_{in} levels, as indicated. For each set of measurements, the BLS collection time, incident light intensity, and other factors that affect the BLS signal level were held constant. The BLS probe point was 3 mm from the input transducer and other MSW pulse conditions were the same as for the microwave measurements.

As indicated by Eq. (2), the measured $I_{BLS}T_D$ vs T_D response is expected to have a characteristic time constant equal to the effective relaxation time for the spin waves that are excited by the MME pulse as it passes the BLS probe point. All of the data in Fig. 4 exhibit the expected form for the transient response, with an initial rise in $I_{BLS}T_D$ as the duty cycle period increases from zero followed by a leveling off at large T_D values. The fact that the data extrapolate to $I_{BLS}T_D=0$ in the $T_D\rightarrow0$ limit indicates that the spin-wave scattering generally dominates and that there is little if any scattering from low-wave-number spin waves associated with the MSW pulse itself. This corresponds to $B=0$ in Eq. (2). The solid line exponential fits shown in Fig. 4 were obtained from Eq. (2) with B set to zero.

The characteristic spin-wave relaxation times evident from the exponential fits in Fig. 4 clearly increase with the input pulse-power level. These exponential response times range from about 0.2 μs for the top graph to more than 4 μs for the bottom graph. The corresponding relaxation rate η_{eff} ranges from around 5×10^6 rad/s for the top graph and $P_{in}=5$ mW to less than 0.3×10^6 rad/s for the lowest graph and $P_{in}=1650$ mW.

The above results are remarkable in several aspects. First, they show that integrated or time-averaged BLS data can be used in combination with a repetitive sequence of narrow

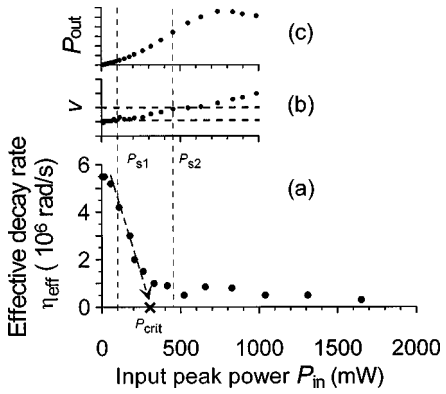

FIG. 5. Graph (a) shows the measured effective spin-wave decay rate η_{eff} as a function of the input peak power P_{in}. Graph (b) and (c) show the velocity and output peak power P_{out} data from Fig. 3. The P_{s1} and P_{s2} thresholds are the same as in Fig. 3. The dashed arrow and P_{crit} point indicate the spin-wave instability threshold power point apparent from the data.

MSW pulse signals launched with different duty cycles to determine experimentally the decay rate of the accessible spin-wave excitations associated with these MSW pulses. Second, the fact that the decay rate obtained for these spin waves in the low-power limit is very close to the intrinsic relaxation rate underscores the validity of the measurement. Third, and most remarkable, is the clear evidence for a rapid decrease in the effective relaxation rate from η_{sw} as the MSW pulse power is increased.

Figure 5 shows results on the P_{in} dependence of the effective spin-wave relaxation rate η_{eff} obtained from a large number of individual data runs of the sort shown in Fig. 4. Graph (a) shows the η_{eff} vs P_{in} results. Graphs (b) and (c) repeat the velocity v and P_{out} vs P_{in} results and the P_{s1} and P_{s2} identifications from Fig. 3. These results are shown again in order to demonstrate clearly the correlations between the soliton response characteristics and the spin-wave decay properties. The dashed arrow and P_{crit} point in (a) show the spin-wave instability threshold power point apparent from the data. The possible origin of this threshold will be considered in Sec. IV.

The rapid falloff in the effective relaxation rate with the input MSW pulse power for the spin waves detected by the BLS system is clearly evident from graph (a) in Fig. 5. It is interesting that this falloff starts even before P_{in} reaches the initial nonlinear threshold P_{s1} point. Recall that this threshold point corresponds to the power at which soliton formation begins. This means that whatever processes are responsible for the drop in η_{eff}, some or all of them are unrelated to soliton formation *per se*.

As P_{in} increases above P_{s1}, the drop in η_{eff} continues at about the same rate of decrease out to about 250–300 mW. The extrapolation of the data from $P_{\text{in}}=P_{s1}=100\,\text{mW}$ to $P_{\text{in}}=250\,\text{mW}$ or so gives a zero decay or $\eta_{\text{eff}}=0$ power point at $P_{\text{crit}}=300\,\text{mW}$. It is suggested in the next section that this P_{crit} point for zero decay corresponds to the Suhl threshold for spin-wave instability. In the conventional high-power microwave experiment, this threshold marks the threshold for the unstable growth of parametrically excited spin waves and the onset of additional microwave loss. In these experiments, the power dependence of the effective decay rate is evident below threshold as one approaches the point at which unstable spin-wave growth occurs.

Finally, the data in Fig. 5 show that as one approaches the $P_{\text{in}}=P_{s2}=450$-mW point, the effective decay rate bottoms out at a value of $0.5-1\times10^6$ rad/s, with a gradual movement to the lower end of this range at the highest powers available for the measurements. These power levels are well into the regime of higher-order soliton formation as well as the nonlinear regime well above the Suhl threshold. Here, one would expect some sort of steady-state nonlinear response. The data suggest a nonlinear spin-wave decay rate that is reduced below the intrinsic relaxation rate by a factor on the order of five to ten.

IV. CONNECTIONS WITH SUHL PROCESSES

As already indicated, the above results on a spin-wave relaxation rate that decreases as the input power increases are somewhat surprising. The initial expectation was that the data would yield a decay rate that reflected the intrinsic spin-wave relaxation rate for the parametrically excited spin waves. The experimental result suggests that the decay depicted in Fig. 4 is not simply this intrinsic relaxation rate η_k. Rather, there is an *effective* decay rate due to the combined effect of the intrinsic relaxation that serves to *reduce* the population of the parametric magnons and the parametric coupling that serves to *increase* the population of these magnons.

Through the spin-wave instability theory developed by Suhl[22] and by Schlömann,[23] one obtains a decay rate for parametrically pumped spin waves given by

$$\eta_{\text{pp}}=\eta_k-G_k^{\min}, \tag{3}$$

where $G_k^{\min}$ is a coupling rate coefficient for the parametric pumping induced energy flow into these modes. The general coupling coefficient G_k is discussed in detail in Ref. 23 and in various extensions of the Schlömann analysis to different geometries, pumping configurations, and anisotropic materials.[26–28]

The main point for this work is that G_k in its most general form represents the coupling of energy from a microwave pump field into spin waves at a particular wave vector $\mathbf{k}$ and frequency ω_k. The more specialized coefficient $G_k^{\min}$ corresponds to that G_k for spin waves at some specific $\mathbf{k}$ and ω_k, which represents the maximum coupling among all of the available spin waves for the given geometry, microwave pumping configuration, and applied magnetic field. For the experiments considered here, $G_k^{\min}$ corresponds to spin waves at $\omega_k=\omega$, where ω is the 5-GHz MSBVW signal frequency. This $G_k^{\min}$ also corresponds to second-order or four-wave processes in which two low–wave-number MSBVW magnons at frequency ω are destroyed and two parametric magnons are created. For such processes, one may show that G_k is proportional to the square of the microwave pumping field amplitude, or equivalently, to the input microwave power. One may write, therefore,

$$G_k^{\min}=Q_k^{\min}P_{\text{in}}, \tag{4}$$

where $Q_k^{\min}$ is a power-independent coupling coefficient.

In the Schlömann spin-wave instability formalism, one assumes a time-dependent spin-wave amplitude of the form

$$b_k \propto e^{-\eta_{pp} t}, \tag{5}$$

where η_{pp} is defined in Eq. (3). One obtains the spin-wave instability threshold power level P_{crit} as the input power at which η_{pp} changes from positive to negative and at which the spin-wave amplitude begins to exhibit an exponential growth characteristic. The condition $\eta_{pp}=0$, in combination with Eqs. (3) and (4), gives a spin-wave instability threshold power,

$$P_{crit} = \eta_k / Q_k^{min}. \tag{6}$$

In the usual microwave spin-wave instability experiment, the threshold P_{crit} is the power at which nonlinear loss becomes apparent. For powers *above* P_{crit}, one sees the effect of the increase in the spin-wave amplitude above thermal levels as an abrupt change in the microwave loss of the sample.

The data in Sec. III and, in particular, the rapid drop in η_{eff} with power shown in Fig. 5 when P_{in} *is less than* P_{crit}, indicate that the effective decay rate obtained from the duty cycle analysis corresponds to the parametric-pumping decay rate η_{pp}. This drop in η_{eff}, therefore, may be taken as an experimental signature for the parametric-pumping process *below* threshold.

$$\eta_{pp} = \eta_{eff} = \eta_k - Q_k^{min} P_{in} \quad (P_{in} < P_{crit}). \tag{7}$$

The dashed arrow in Fig. 5 is intended to indicate this basic response. The slope for this decrease corresponds to the Q_k^{min} factor defined above.

The present results represent the first direct demonstration that the parametric-pumping process actually serves to *decrease* the effective spin-wave relaxation rate for power levels *below* the instability threshold. The role of such parametric pumping processes in nonlinear MSW devices, such as the magnetostatic surface wave signal-to-noise enhancer,[29] for example, is well known. However, all previous data on spin-wave instability processes show only the effect of the parametric pumping *above* threshold, when the pumped spin waves become unstable.

Turn now to the η_{eff} results at the highest powers available for the measurements. Based on spin-wave instability considerations alone, one would expect η_{eff} to follow the dashed arrow in Fig. 5(a) all the way to $\eta_{eff}=0$ at the threshold power point $P_{in}=P_{crit}$. The data, however, show that the effective decay rate levels off at a small but nonzero value. This leveling off occurs when the input power level approaches and exceeds the threshold P_{s2} for complete order one soliton formation at the BLS probe point. One may speculate that when the order one soliton power threshold is exceeded, the additional microwave energy that is provided to the initial nonlinear MSW pulse as it is launched from the input transducer must eventually be shed through the generation of spin waves. The order one soliton is a fully formed propagating nonlinear eigenmode of the system. The additional energy that feeds this pulse above the P_{s2} threshold must go somewhere. Both the wave-vector selective BLS experiments in Ref. 19 and the present decay results indicate that this energy goes into spin waves that are pumped by the nonlinear MSW pulse.

The empirical connection between the behavior of η_{eff} in Fig. 5 and the form of η_{pp} in Eqs. (3) and (7) notwithstanding, one critical problem remains. The parametric pumping of spin waves in the Suhl and Schlömann analyses give a power-dependent spin-wave decay rate of the form shown in Eq. (3) *during* the time that microwave power is being applied to the spin system. In the present experiments, the input pulse microwave power generates propagating MSW pulses in the YIG film, and the dynamic magnetization associated with these propagating pulses generates the spin waves observed by light scattering in Ref. 19 and as described above. In these instances, the observed decay in the spin-wave signal takes place mostly *after* the passage of the nonlinear MSW generating pulse. The dilemma here is clear. How does the decaying spin-wave remember its parametric origin in the propagating MSW pulse?

Further BLS measurements of the fundamental spin-wave decay processes presented above will be needed in order to address the above question. It will be important to obtain time and spatially resolved measurements of the actual spin-wave decay following the techniques of Ref. 20, but with the addition of wave-vector selection procedures from Ref. 19. These techniques will allow one (i) to follow the spin-wave decay in time at a fixed BLS probe point as the generating MSW pulse moves by, (ii) to follow the spatial decay at fixed time as one moves away from a specific generation point in time and position, and (iii) to identify the specific critical spin-wave modes that are excited.

It is expected that the details of the decay processes revealed by these new measurements will differ from those for Suhl processes alone and direct parametric spin-wave excitation from a continuous MSW signal or microwave pump. These later processes are already well documented.[30–40] These differences will provide additional insight into the parametric spin-wave processes associated with MSW pulse or soliton excitation.

ACKNOWLEDGMENTS

This work was supported by the National Science Foundation, Grants No. DMR-9400276 and No. DMR-9801649, and the United States Army Research Office, Grants No. DAAHO4-95-1-0325 and No. DAAG55-98-1-0430. The samples were provided by Dr. J. D. Adam, Northrop Grumman Science and Technology Center, Pittsburgh, PA. Dr. Valeri T. Synogach and Dr. Christoph Mathieu are acknowledged for a critical review of the manuscript.

*Present address: Department of Chemistry, Colorado State University, Fort Collins, CO 80523.

†On leave from the Faculty of Electrical Engineering and Information Technology, Slovak Technical University, Bratislava, Slovakia. Present address: National Institute of Standards and Technology, Boulder, CO 80303.

‡Present address: Department of Physics, The Ohio State University, Columbus, OH 43210.

§Present address: P&H Laboratories, Simi Valley, CA 93063.

[1] B. A. Kalinikos, N. G. Kovshikov, and A. N. Slavin, Pis'ma Zh.

Eksp. Toer. Fiz. **38**, 343 (1983) [JETP Lett. **38**, 413 (1983)].
[2] P. De Gasperis, R. Marcelli, and G. Miccoli, Phys. Rev. Lett. **59**, 481 (1987).
[3] B. A. Kalinikos, N. G. Kovshikov, and A. N. Slavin, IEEE Trans. Magn. **28**, 3207 (1992).
[4] M. Chen, M. A. Tsankov, J. M. Nash, and C. E. Patton, Phys. Rev. B **49**, 12 773 (1994).
[5] M. A. Tsankov, M. Chen, and C. E. Patton, J. Appl. Phys. **76**, 4274 (1994).
[6] N. G. Kovshikov, B. A. Kalinikos, C. E. Patton, E. S. Wright, and J. M. Nash, Phys. Rev. B **54**, 15 210 (1996).
[7] H. Xia, P. Kabos, C. E. Patton, and H. E. Ensle, Phys. Rev. B **55**, 15 018 (1997).
[8] M. Chen, M. A. Tsankov, J. M. Nash, and C. E. Patton, Phys. Rev. Lett. **70**, 1707 (1993).
[9] A. N. Slavin, IEEE Trans. Magn. **31**, 3479 (1995).
[10] J. M. Nash, C. E. Patton, and P. Kabos, Phys. Rev. B **51**, 15 079 (1995).
[11] H. Xia, P. Kabos, R. A. Staudinger, C. E. Patton, and A. N. Slavin, Phys. Rev. B **58**, 2708 (1998).
[12] J. M. Nash, P. Kabos, R. Staudinger, and C. E. Patton, J. Appl. Phys. **83**, 2689 (1998).
[13] H. Y. Zhang, P. Kabos, H. Xia, R. A. Staudinger, P. A. Kolodin, and C. E. Patton, J. Appl. Phys. **84**, 3776 (1998).
[14] R. A. Staudinger, P. Kabos, H. Xia, B. T. Faber, and C. E. Patton, IEEE Trans. Magn. **34**, 2334 (1998).
[15] B. A. Kalinikos, N. G. Kovshikov, and C. E. Patton, Phys. Rev. Lett. **78**, 2827 (1997).
[16] B. A. Kalinikos, N. G. Kovshikov, and C. E. Patton, Phys. Rev. Lett. **80**, 4301 (1998).
[17] A. V. Bagada, G. A. Melkov, A. A. Serga, and A. N. Slavin, Phys. Rev. Lett. **79**, 2137 (1997).
[18] P. A. Kolodin, P. Kabos, C. E. Patton, B. A. Kalinikos, N. G. Kovshikov, and M. P. Kostylev, Phys. Rev. Lett. **80**, 1976 (1998).
[19] H. Xia, P. Kabos, H. Y. Zhang, P. A. Kolodin, and C. E. Patton, Phys. Rev. Lett. **81**, 449 (1998).
[20] M. Bauer, O. Büttner, S. O. Demokritov, B. Hillebrands, Y. Grimalsky, Yu. Rapaport, and A. N. Slavin, Phys. Rev. Lett. **81**, 3769 (1998).
[21] P. Kabos, C. E. Patton, G. Wiese, A. D. Sullins, E. S. Wright, and L. Chen, J. Appl. Phys. **80**, 3962 (1996).
[22] H. Suhl, J. Phys. Chem. Solids **1**, 209 (1957).
[23] E. Schlömann, Research Division, Raytheon Company Technical Report No. R-48, 1959 (unpublished).
[24] R. W. Damon and J. R. Eshbach, J. Phys. Chem. Solids **19**, 308 (1961).
[25] Interferometer system manufactured by JRS, Ltd., Zwillikerstrasse 8, 8910 Affoltern a. A., Switzerland.
[26] C. E. Patton, J. Appl. Phys. **40**, 2837 (1969).
[27] C. E. Patton, Phys. Status Solidi B **92**, 211 (1979).
[28] C. E. Patton, Phys. Status Solidi B **93**, 63 (1979).
[29] S. N. Stitzer and P. R. Emtage, Circuits Syst. Signal Process. **4**, 228 (1985).
[30] G. Wiese, Z. Phys. B: Condens. Matter **91**, 57 (1993).
[31] C. E. Patton, in *Magnetic Oxides*, edited by D. J. Craik (Wiley, London, 1975), pp. 575–645.
[32] C. E. Patton and W. Jantz, J. Appl. Phys. **50**, 7082 (1979).
[33] G. Wiese, P. Kabos, and C. E. Patton, J. Appl. Phys. **74**, 1218 (1993).
[34] G. Wiese, P. Kabos, and C. E. Patton, Phys. Rev. B **51**, 15 085 (1995).
[35] W. Wettling, W. D. Wilber, P. Kabos, and C. E. Patton, Phys. Rev. Lett. **51**, 1680 (1983).
[36] P. Kabos, C. E. Patton, and W. D. Wilber, Phys. Rev. Lett. **53**, 1962 (1984); **54**, 851(E) (1985).
[37] W. D. Wilber, W. Wettling, P. Kabos, C. E. Patton, and W. Jantz, J. Appl. Phys. **55**, 2533 (1984).
[38] W. D. Wilber, J. G. Booth, C. E. Patton, G. Srinivasan, and R. W. Cross, J. Appl. Phys. **64**, 5477 (1988).
[39] P. Kabos, G. Wiese, and C. E. Patton, Phys. Rev. Lett. **72**, 2093 (1994).
[40] P. Kabos, M. Mendik, G. Wiese, and C. E. Patton, Phys. Rev. B **55**, 11 457 (1997).